Investigation on the Effect of Variation in Cutting Speeds and Angle of Cut During Slant Type Taper Cutting in WEDM of Hastelloy X

I. V. Manoj, Ranjit Joy & S. Narendranath

Arabian Journal for Science and Engineering

ISSN 2193-567X
Volume 45
Number 2

Arab J Sci Eng (2020) 45:641-651
DOI 10.1007/s13369-019-04111-2

Springer

Arabian Journal for Science and Engineering (2020) 45:641–651
https://doi.org/10.1007/s13369-019-04111-2

RESEARCH ARTICLE - MECHANICAL ENGINEERING

Investigation on the Effect of Variation in Cutting Speeds and Angle of Cut During Slant Type Taper Cutting in WEDM of Hastelloy X

I. V. Manoj[1] · Ranjit Joy[1] · S. Narendranath[1]

Received: 26 March 2019 / Accepted: 10 September 2019 / Published online: 17 September 2019

Abstract

Nickel-based superalloys are classified under difficult to machine materials due to its higher affinity to tool materials and low thermal diffusivity. Wire electric discharge machining (WEDM) is a spark eroding technique for precise machining of such superalloys with complex machining geometries. Tapering in WEDM has many disadvantages like wire break, angular inaccuracies and dielectric distribution for better surfaces. In this paper, a unique method was developed and employed to achieve taper surface by tilting the workpiece using a slant type taper fixture for machining of tapered surfaces. Different aspects like cutting thickness, surface roughness, slant angle, surface crack density and width of cut were examined for five distinct cutting speed parameters at different angles, namely 0°, 15°, 30°, 45° and 60°. In the present research work, Hastelloy X was machined using zinc-coated copper wire and cutting speed was ranged between 0.16 and 2.49 mm/min. The slant angle was observed to be independent of cutting speed, and it was influenced by wire vibration, manufacturing imprecisions of slant fixture. It was found that as the cutting speed increases, surface crack density and surface roughness also increase. It was observed that both the parameters increased with the increase in the angle of cut from 0° to 60° although the cutting speed decreased.

Keywords Taper cutting · Slant type taper fixture · Hastelloy X · Angular error · Surface roughness · Surface crack density

1 Introduction

Superalloys are an amalgamation of different metals which have good mechanical properties like excellent mechanical strength, resistance to thermal creep deformation, good surface stability and resistance to corrosion or oxidation. Nickel-based superalloys have an austenitic matrix which is subjected to work harden rapidly during machining. The presence of nickel leads to different adverse properties like affinity to react with the tool materials and low thermal diffusivity which makes the machining operation more difficult and challenging. These alloys are widely used in the manufacture of various components and structures for aerospace, marine and nuclear power generation, chemical, petrochemical and process industries [1–3].

Traditional machining techniques are unadaptable for machining of nickel-based alloys, as it not only leads to damage of the work surface but also causes tool failure. In numerous non-traditional machinings like abrasive water jet machining, laser machining, electrochemical machining and electric discharge machining, WEDM is one of the most preferred machining techniques for machining of such difficult to machine materials with precise complex profiles [4]. Shihab [5] has performed optimization and prediction in the machining of friction stir welded 5754 aluminium alloy using WEDM considering process parameters such as pulse on time, pulse off time and peak current. The Box–Behnken design of the response surface methodology was employed in the study to examine material removal rate, surface roughness and kerf width. Goswami and Kumar [6] have investigated the machining of nimonic 80A with the brass wire electrode, where the pulse on time has influenced surface roughness and material removal rate. Soni et al. [7] examined the surface crack density in WEDM of shape memory alloy; it was reported that as the cutting speed increases the surface crack density and surface roughness were also increased. Zhang et al. [8] have developed mathematical predictive models for surface crack density in the machining of tungsten tool YG15 by WEDM. It was reported that pulse

✉ I. V. Manoj
vishalmanojvs@gmail.com

[1] Department of Mechanical Engineering, National Institute of Technology Karnataka, Surathkal 575025, India

on time and pulse current are the most significant factors influencing surface crack density.

The tapering process can generate curved surfaces on the workpiece which can be easily machined with the WEDM process by bending the electrode to the required angle. From the literature, different problems related to tapering in WEDM and various methods that were adopted to achieve taper using WEDM were highlighted. Many simulations and prediction models have been formulated for the prediction of angular errors. Selvakumar et al. [9] have investigated grey relational analysis in optimizing the process parameters involved during tapering of AISI D3 tool steel with the aid of WEDM. It was found that cutting speed was independent of angular error, and taper accuracy was most influenced by wire tension and taper angle. Martowibowo and Wahyudi [10] have implemented the Taguchi method in taper motion WEDM; it was observed that pulse on time and taper angle influenced material removal rate and surface roughness. Kinoshita et al. [11] have highlighted many drawbacks of taper machining in WEDM like deflection of wire, fluctuations in tension, insufficient flushing and wire breakage due to uneven forces acting on the wire. A unique wire guide system was developed to counter those problems and to improve the accuracies of taper. Plaza et al. [12] have formulated prediction models to predict angular error, where part thickness and taper angle were considered to be the most influential factors. By using this design of experiment-based model, not only the experiments were reduced but also angular errors were minimized. Sanchez et al. [13] have formulated a quadratic equation considering electrical parameters with part geometry and FEM model simulation. The FEM model involved the mechanical behaviour of wire with nonlinear phenomena such as contact mechanics, plastic behaviour and stress stiffening for prediction of angular error. It was reported that taper deviations would be reduced by less than 0°4′ using the models. Sanchez et al. [14] simulated WEDM taper cutting which predicted the angular error considering friction effects for large angles and reducing trial experimentation for investigating the errors. It was reported that angular error for a machining situation depends on wire material, part material, thickness and several other electrical parameters like on-time, off-time and open-circuit voltage. Yan et al. [15] have reported two types of six-bar linkage mechanism models for tapering in WEDM. The first mechanism produced taper parts with only angular error but no transverse guider wear, and the second mechanism produced only wear between transverse guider and wire electrode but no angular error while machining. The mechanism that produced angular error but no wear was adopted, and a new intelligent model was also proposed to improve accuracy, reduce friction and wear between guide and electrode. A strategy was proposed to control discharge power and wire tension in order to track the material removal around corners including interfaces which could stop the feed rate surge. This would retain accurate shape which was employed in the machining of conjugate root gear and turbine blades with tapering in WEDM.

In the present research work, tapering was performed on Hastelloy X with the aid of an in-house developed novel slant type taper fixture, which eliminates most of the limitations during taper machining in WEDM. Although there were many methods and models that were used to achieve the tapering process, many problems like wire break, angular error, guide wear and surface flaws were found to be inevitable. These problems occur primarily because of the fact that in most of the cases the wire is subjected to bending at the required angle to achieve taper. The slant type fixture enables to generate taper by bending the workpiece during machining without disturbing the wire or wire guide. The effects of variation in cutting speed and angle of cut on cutting thickness, surface roughness, angular error, surface crack density and kerf width were emphasized during slant type taper machining. The workpiece was cut in different angles, namely 0°, 15°, 30°, 45° and 60° with the help of the slant angle achieved by the fixture.

2 Materials and Methods

2.1 Work Material

Hastelloy X (Alloy X) is a nickel–chromium–iron–molybdenum alloy which can be used in many high-temperature applications such as gas turbine's exhaust and the combustion zones, tailpipes of aircraft, spray bars, flame holders, afterburners and cabin heaters. It is difficult to precisely machine the alloy which has such applications having a taper and complex geometry. WEDM is a high-precision machining technique for machining such electrically conductive hard materials. Hastelloy X material was received in the form of a plate of dimensions $250 \times 250 \times 10$ mm. It was subjected to energy-dispersive X-ray analysis (EDX) for confirmation of its composition, and it is reported in Fig. 1. Before machining, the as-received alloy was heat treated to full annealing by heating at 1175 °C for 1 h as established from literature [16]. This relieves the stresses in the alloy before machining for ensuring minimal residual stress to avoid distortion.

2.2 Experimental Details

The experiments were performed in Electronica 'ELPLUS 15 CNC WEDM'. The electrode material zinc-coated copper wire of 0.25 mm diameter was used throughout the experiment using deionized water as the dielectric fluid. In WEDM process, the wire and the workpiece are maintained at high

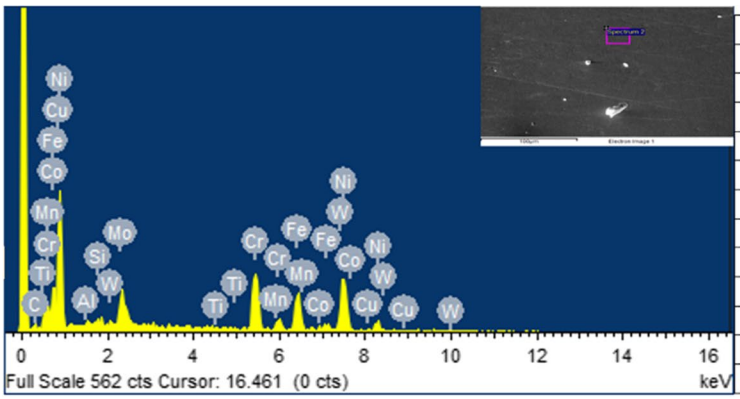

Element	Weight%
C	7.75
Al	0.41
Si	0.11
Ti	0.13
Cr	18.33
Mn	0.75
Fe	17.34
Co	0.48
Ni	44.53
Cu	1.41
Mo	7.83
W	0.95

Fig. 1 EDAX analysis of Hastelloy X

voltage difference, where the wire cuts the workpiece due to local melting created by sparks. The dielectric fluid provides an instant cooling effect and also clears the debris due to the flushing effect making way for the wire to proceed. In the current work based on different machining parameters, Hastelloy X was cut at various angles. The machining was carried out by tilting the workpieces at different standard angles using a slant type fixture as shown in Fig. 2a. The slant type fixture was fixed to the WEDM bed. Figure 2b shows how the workpiece was machined at different angles to achieve angular machining in WEDM. During the slant type taper cutting, the workpiece is placed on the angular plate of slant fixture that was mounted on WEDM. The angular plate was tilted and fixed to the side plate slots for required angles namely 0°, 15°, 30°, 45° and 60°. As the angle increases, the cutting thickness also increases and these cutting thickness (t) values can be calculated using cosine function with a known angle of cut and workpiece thickness (10 mm).

2.3 Measurement of Performance Characteristics

In the current study, the cutting speed was recorded from the WEDM machine for each instance and the average values were considered for the angular machining. The angular cut samples were subjected to a hot air blower to remove the moisture. The machined components were measured for angular accuracy using 'TESA VISIO 200' coordinate measuring machine. The surface roughness of angular components was measured using 'Mitutoyo SJ-301' surface roughness tester. The surface crack density and width of cut were measured by employing scanning electron microscopes of 'ZEISS SIGMA' and 'JEO JSM-6368OLA'. The surface crack density is the average crack length per area

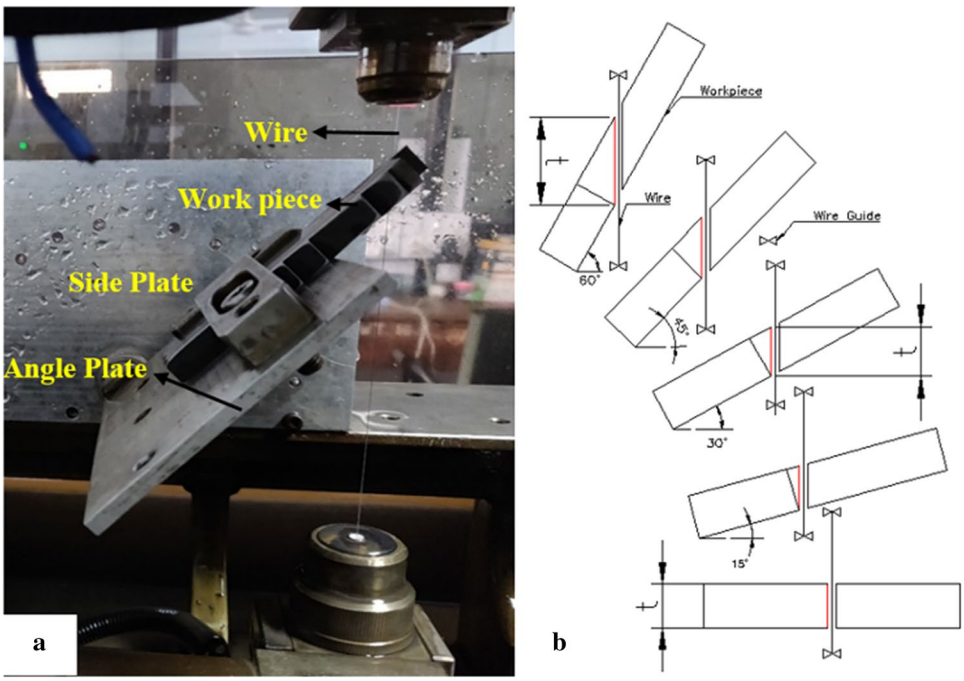

Fig. 2 **a** Slant type taper fixture **b** slant cut at different angles

of the machined surface. The SEM micrographs of 5000× were recorded at upper, lower and at middle zones of angular machined surfaces. The average crack length was measured by the aid of image J software from SEM micrographs.

2.4 Machining Parameters

The machining parameters were chosen through initial experiments conducted on the workpiece material. The power pulse mode (pulse current 12A) and pulse off time of 44µs were set throughout the experiment. Table 1 shows the parameters employed for machining. All the angular machining was carried out at wire guide distance 140 mm from 0° to 60° angles. The parameters were selected based on the machining range of workpiece and tool combination. Table 2 represents Taguchi's L_9 experiment that was performed at different angles with various machining parameters such as pulse on time, servo voltage, wire feed and servo feed. The cutting speeds were recorded, and five distinct cutting speed parameters were chosen from each angle, ranging from the smallest to the largest cutting speeds. The parameters of the five distinct cutting speeds that were chosen for machining are as shown in Table 3. These parameters were used to machine the Hastelloy X at different taper or slant angles to obtain the tapered surface of 5 mm thickness as shown in Fig. 3.

3 Results and Discussion

3.1 Variation of Cutting Speed with Different Angles of Cut

Based on the parameters decided from the initial experiments, the slant type taper machining of Hastelloy X was carried out. It was observed that the cutting speed ranged from 0.16 to 2.49 mm/min for different parameters and at various angles. The variation in cutting speed with a change in the angle of cut is shown in Table 4. The cutting speed increased from trial 1 to trial 5 in all the angles of cut as the pulse on time increased. It can be observed that although trials 2, 3 and trials 4, 5 had the same pulse on time, the decrease in servo voltage increases the cutting speed due to an increase in discharge energy. According to initial experiments, it can be observed that as the pulse on time increases the discharge energy also was increased due to an increase in the intensity of sparks, but in the case of servo voltage, increase in servo voltage increases the spark gap. This reduces the number of sparks striking the workpiece decreasing the discharge energy. Similar trends were observed by Sharma et al. [17] for the machining of nickel-based alloy. The cutting speed is influenced by sparking conditions which are controlled by parameters like pulse duration, workpiece orientation, servo voltage, wire diameter and dielectric [18, 19]. Trial 1 recorded the lowest cutting speed of 0.16 mm/min at 60° slant angle, and trial 5 yielded the maximum speed of 2.49 mm/min at 0° slant angle. Trail 5 had a noticeable increase of 79.15% in cutting speed from trial 4 at 0° due to the increased discharge energy. The cutting speed has been defined as the length of the sample to the time taken to cut by Azam et al. [20]. Figure 4 shows the decrease in cutting speed with an increase in the angle of cut for the chosen machining parameters. This reduction in cutting speeds was observed due to an increase in the length of cutting thickness with increasing angle of cut. For the specifically chosen parameter, as the angle of cut gets increased,

Table 1 Machining parameters

Wire diameter (µm)	250
Wire material	Zinc-coated copper wire
Dielectric fluid	Deionized water
Polarity	Positive
Peak current (A)	12
Pulse on time (µs)	105,115,125
Servo voltage (V)	40,50,60
Wire feed (m/min)	6,7,8
Servo feed (mm/min)	10,15,20
Pulse off time (µs)	44
Wire guide distance (mm)	140

Table 2 Taguchi's L_9 design

Sl. no.	Pulse on time (µs)	Servo voltage (V)	Wire feed (m/min)	Servo feed (mm/min)
1	105	40	6	10
2	105	50	7	15
3	105	60	8	20
4	115	40	7	20
5	115	50	8	10
6	115	60	6	15
7	125	40	8	15
8	125	50	6	20
9	125	60	7	10

Table 3 Parameters of cutting speed

Sl. no.	Pulse on time (µs)	Servo voltage (V)	Wire feed (m/min)	Servo feed (mm/min)
1	105	60	8	20
2	115	50	8	10
3	115	40	7	20
4	125	50	6	20
5	125	40	8	15

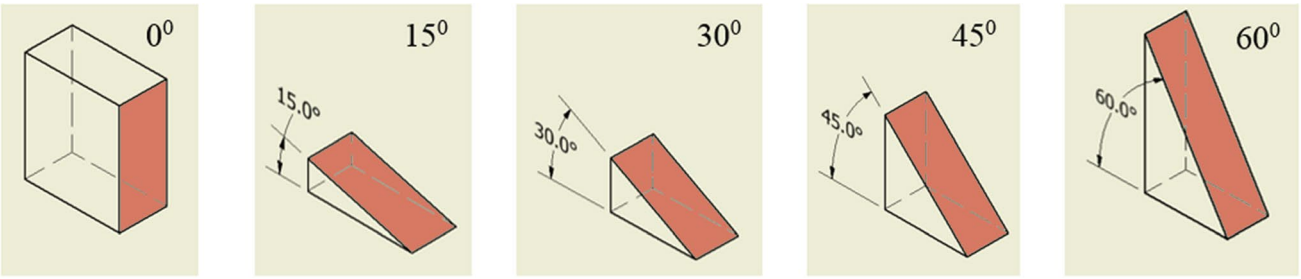

Fig. 3 Taper cut samples at varying angle of cut

Table 4 Cutting speeds at different angles of cut

Trial no.	Pulse on time (μs)	Servo voltage (V)	Wire feed (m/min)	Servo feed (mm/min)	Cutting speed (mm/min)				
					0°	15°	30°	45°	60°
1	105	60	8	20	0.47	0.36	0.33	0.26	0.16
2	115	50	8	10	0.67	0.60	0.52	0.44	0.28
3	115	40	7	20	0.92	0.81	0.70	0.57	0.38
4	125	50	6	20	1.39	1.30	1.23	0.83	0.67
5	125	40	8	15	2.49	1.94	1.62	1.16	0.85

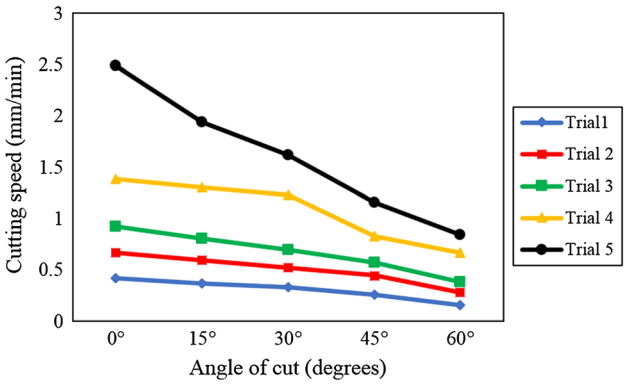

Fig. 4 Variation of cutting speeds with different angles of cut

Table 5 Dead errors on slant type taper fixture

Angle in degrees	CMM angle of the fixture (°)	Dead angular error (°)
0°	00°28′30″	28′30″
15°	15°12′01″	12′01″
30°	29°59′52″	−00′08″
45°	45°00′08″	00′08″
60°	60°04′48″	04′48″

the cutting thickness also increases. This causes an increase in the area for melting compared to a straight cut, as the melting of workpiece takes more time for the same sparking conditions which results in decreasing cutting speeds [19].

3.2 Variation of Angle Error with Cutting Speed

There are a different variety of errors in machining; the dead errors are constant errors which could be either positive or negative and will always contribute to the angular error. The slant type fixture was measured for angular dead errors before machining. Table 5 shows dead angular errors that were measured for different angles. The angular error is the difference in machined angle and the true angle. The actual machined angle can be obtained by deducting the dead errors from CMM measured angle, and angular error was calculated with the help of Eq. (1) and (2) [21]. Table 6 shows the actual error that the sample carries after machining by using slant type taper fixture. Figure 5 shows the behaviour of angular error at different cutting speed parameters for the various angles of cut. Each angle was machined using five different chosen machining parameters. These parameters with different cutting speeds influenced the amplitude of wire vibration as observed by Habib et al. [22]. The machining was not always performed at the mid-span of the wire length due to tilt; there would be a change in vibrational forces and flushing conditions as observed by Habib et al. [23]. Due to this change, the vibrational amplitude of wire a range of errors was caused. The other trails were also used for cutting slant workpieces. Trial 5 was observed to have maximum and minimum errors among all the angle of cut. This parameter gave minimum errors at 0°, 30°, 45° and 60° and maximum error at 15°. It can be observed that at 60° slant angle of cut, there was a change in angular error from positive to negative (−0′53″) for trial 5. This behaviour in

Table 6 Variation of angular error using different machining parameters

True angle (degrees)	Trial no.	Measured angle (°)	Dead error (°)	Actual angle (°)	Angular error (°)
0°	1	0°03′19″	28′30″	−0°26′49″	−26′49″
	2	0°05′50″	28′30″	−0°23′20″	−23′20″
	3	0°02′48″	28′30″	−0°26′18″	−26′18″
	4	0°06′25″	28′30″	−0°23′55″	−23′55″
	5	0°09′17″	28′30″	−0°19′20″	−19′20″
15°	1	14°49′56″	12′01″	14°37′55″	−22′05″
	2	14°45′52″	12′01″	14°33′51″	−26′09″
	3	14°46′56″	12′01″	14°34′55″	−25′05″
	4	14°44′54″	12′01″	14°32′53″	−27′07″
	5	14°42′34″	12′01″	14°30′33″	−29′27″
30°	1	30°08′27″	−00′08″	30°08′35″	08′35″
	2	30°04′40″	−00′08″	30°04′48″	04′48″
	3	30°10′53″	−00′08″	30°11′01″	11′01″
	4	30°10′22″	−00′08″	30°10′30″	10′30″
	5	30°01′29″	−00′08″	30°01′37″	01′37″
45°	1	45°17′45″	00′08″	45°17′37″	17′37″
	2	45°20′47″	00′08″	45°20′39″	20′39″
	3	45°19′46″	00′08″	45°19′38″	19′38″
	4	45°18′38″	00′08″	45°18′30″	18′30″
	5	45°09′59″	00′08″	45°09′51″	09′51″
60°	1	60°09′09″	04′48″	60°03′21″	3′21″
	2	60°07′10″	04′48″	60°03′32″	3′32″
	3	60°12′08″	04′48″	60°07′20″	7′20″
	4	60°10′04″	04′48″	60°05′16″	5′16″
	5	60°03′55″	04′48″	59°59′07″	−0′53″

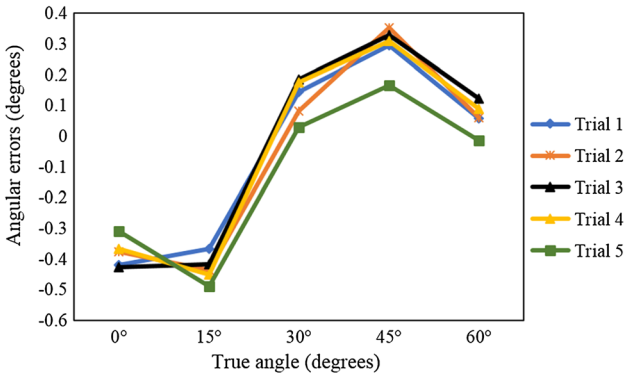

Fig. 5 Variation of angular error with different cutting speed parameters

angular error was due to the maximum vibrational amplitude that occurs at the highest discharge frequency and at higher cutting thickness [19, 24]. These vibrational amplitudes may increase or decrease the angular error during slant type taper machining. The kerf width for trial 5 was also observed to be the highest as stated in Sect. 3.5. From Fig. 5, the error was observed to be shifted from negative to positive from 15° to 30° and this shift was noticed due to the manufacturing errors and stochastic wire vibration [24]. The angular accuracy was found to be influenced by wire vibration and wire tension as reported by Selvakumar et al., but it is independent of cutting speed [9].

$$\text{Actual angle} = \text{CMM angle} - \text{Dead error} \quad (1)$$

$$\text{Angular Error} = \text{Actual angle} - \text{True Angle} \quad (2)$$

3.3 Variation of Surface Roughness with Cutting Speed for Different Angles of Cut

The surface roughness is a vital parameter that can be used as a measure of surface integrity. Table 7 shows the variation of surface roughness for varying cutting speeds. Figure 6 shows the trends of surface roughness with cutting speed at different angles of cut. It was observed that as the cutting speed increases the surface roughness also increases. The surface roughness of the machined surface was 3.57 µm at the highest cutting speed of 2.49 mm/min at 0° and 1.73 µm at the lowest cutting speed of 0.16 mm/min at 60°. During WEDM, the surface roughness was due to the craters produced on the machined surface by the spark to melt

Table 7 Surface roughness observed for varying cutting speed and angle of cut

Trial no.	0°		15°		30°		45°		60°	
	CS (mm/min)	SR (μm)	CS (mm/min)	SR (μm)	CS (mm/min)	SR (μm)	CS (mm/min)	SR (μm)	CS (mm/min)	SR (μm)
1	0.47	1.79	0.36	1.88	0.33	1.95	0.26	1.75	**0.16**	**1.73**
2	0.67	2.90	0.60	2.8	0.52	2.18	0.44	2.3	0.28	2.58
3	0.92	3.11	0.81	2.99	0.70	2.75	0.57	2.96	0.38	2.64
4	1.39	3.49	1.30	3.81	1.23	3.58	0.83	3.83	0.67	3.71
5	**2.49**	**3.57**	1.94	3.85	1.62	3.93	1.16	3.95	**0.85**	**3.99**

CS cutting speeds, *SR* surface roughness

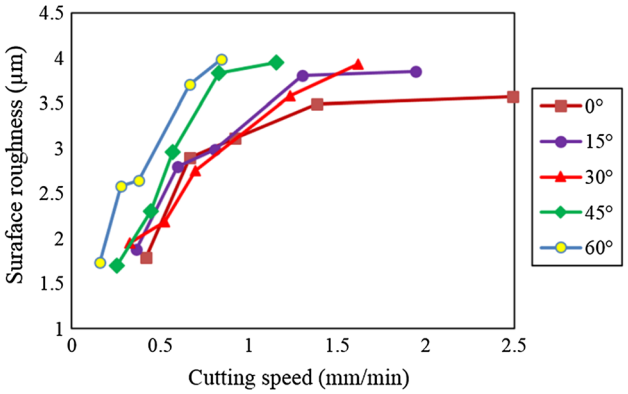

Fig. 6 Variation of surface roughness with different cutting speeds

the workpiece reported by Sharma et al. [17]. The surface roughness was found to be influenced by pulse on time and servo voltage. The increase in pulse on time leads to a higher intensity of sparks causing more craters which increase the surface roughness of the machined angular surface. The increase in sparks also increases the discharge energy which offers higher cutting speeds in the machining of the material. But in the case of servo voltage, as it increases the spark gap between electrode and material becomes more, it reduces the number of sparks hitting the workpiece [17, 25]. Therefore, there is a decrease in the discharge energy reducing the number of craters with a decrease in cutting speed. Figure 7 shows SEM micrograph at lowest and highest cutting speeds. Figure 7a shows reduced micro-holes and micro-globules due to the lowest discharge energy with the lowest cutting speed on the machined surface. Figure 7b shows the SEM images for the machined angular surface at highest discharge energy with the highest cutting speed having more number of micro-craters, micro-globules and micro-holes which contributes to higher surface roughness. The highest surface roughness was measured to be 3.99 μm for cutting speed of 0.18 mm/min at 60°. This increase in surface roughness at lower cutting speed was due to the high cutting thickness that was due to an increase in the angle of cut. This behaviour was observed due to the increased discharge energy and the variation in gap voltage at trial 5. However, similar results as reported by Samanta et al. [19] for varying job height condition during WEDM.

3.4 Variation of Surface Crack Density with Cutting Speed

Table 8 shows the calculated surface crack density for different cutting speeds at a various angles of cut. It was observed from Fig. 8 that as the cutting speed increases the surface crack density also increases. It was calculated that surface crack density at highest cutting speed of 2.49 mm/min was 0.257 μm/μm^2 at slant angle 0° and at lowest cutting speed of 0.16 mm/min the surface crack density was 0.328 μm/μm^2 at 60°. During WEDM process, there are instantaneous

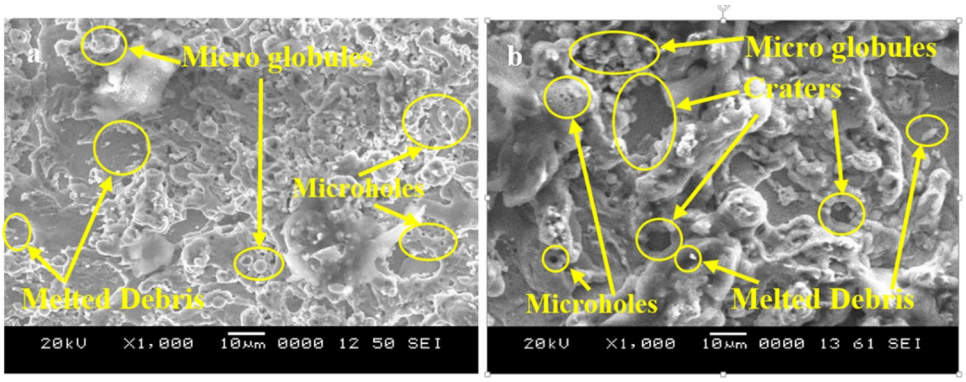

Fig. 7 SEM micrographs of **a** lowest cutting speed at slant angle of 60° **b** highest cutting speed at slant angle of 0°

Table 8 Surface crack density at different cutting speeds for various angles of cut

Trial no.	0°		15°		30°		45°		60°	
	CS (mm/min)	SCD (μm/μm^2)	CS (mm/min)	SCD (μm/μm^2)	CS (mm/min)	SCD (μm/μm^2)	CS (mm/min)	SCD (μm/μm^2)	CS (mm/min)	SCD (μm/μm^2)
1	0.47	0.188	0.36	0.218	0.33	0.256	0.26	0.293	**0.16**	**0.328**
2	0.67	0.197	0.60	0.231	0.52	0.269	0.44	0.312	0.28	0.349
3	0.92	0.207	0.81	0.241	0.70	0.282	0.57	0.322	0.38	0.370
4	1.39	0.233	1.30	0.264	1.23	0.298	0.83	0.338	0.67	0.386
5	**2.49**	**0.257**	1.94	0.293	1.62	0.339	1.16	0.395	**0.85**	**0.455**

CS cutting speeds, *SCD* surface crack density

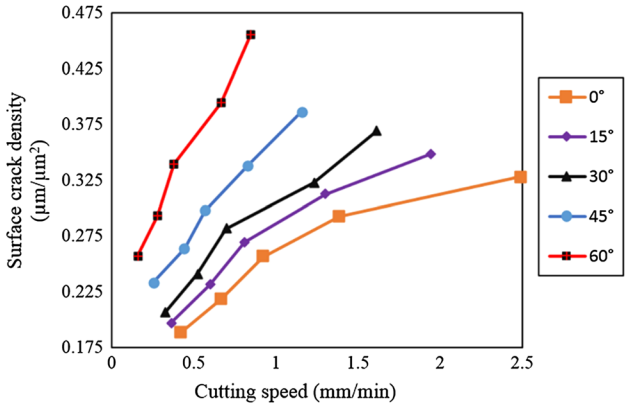

Fig. 8 Variation of surface crack density with different cutting speeds

heating/cooling cycles of the workpiece that arises due to the melting and flushing of dielectric at cutting region. This rapid heating and cooling continuous cycles lead to the formation of thermal stress on the machined surface. These thermal stresses on the surface cause cracks which may lead to failure of the component [26]. With the increase in cutting speeds, the number of heating and cooling cycle's increases leading to more thermal stress, causing more cracks. Hence, the surface crack density increases with an increase in cutting speed as observed by Soni et al. [7]. The highest surface crack density was calculated as 0.455 μm/μm^2 at 60° for cutting speed of 0.85 mm/min. From Fig. 8, it can be observed that the surface crack density increased although the cutting speed decreased with an increase in the angle of cut. As the angle of cut increases, the cutting thickness also increases. The cutting thickness increase was calculated to be 41.42% from 45° to 60° and 22.47% from 30° to 45° slant angles which were highest compared to other angles of cut. With an increase in cutting thickness, the area that is required to melt is also increasing. As the surface area of angular machined part that is subjected to heating and cooling cycle increases, it induces more cracks due to increased thermal stress, although there is a decrease in cutting speed making curve linear in Fig. 8 comparing the 60° to 0° curve [8]. Figure 9a, b shows the SEM images with cracks for angular specimens at 0° and 60° for the highest cutting speeds at respective angles. The larger micro-cracks are observed in Fig. 9a, i.e., in the machined surface at 0°. Figure 9b shows smaller and deeper micro-cracks at 60° angular machined surfaces in higher magnifications.

3.5 Variation of the Width of Cut for Different Angles of Cut

The width of cut is also known as kerf width and is the distance of cut perpendicular to the direction of the wire path in WEDM. The different width of cut that was measured by

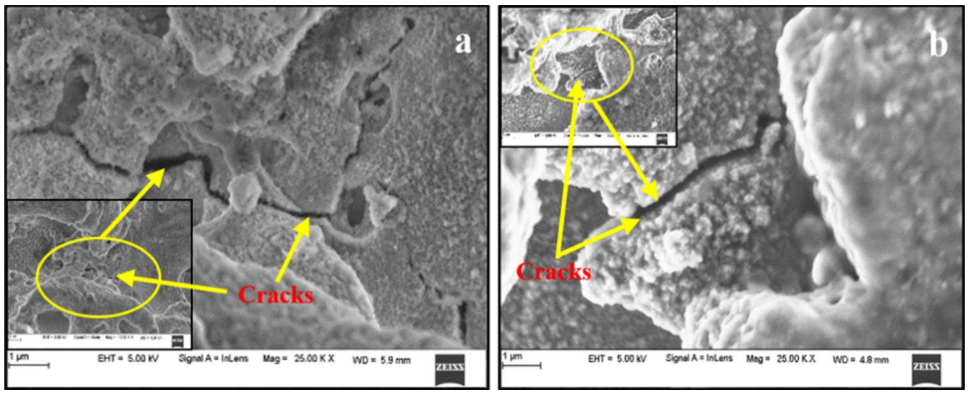

Fig. 9 SEM images of angular cut specimen at **a** highest cutting speed at 0° **b** lowest cutting speed at 60°

Table 9 Width of cut observed for different slant angles for various cutting parameters

Trial no.	Width of cut (μm)				
	0°	15°	30°	45°	60°
1	**280.678**	305.789	318.642	332.375	**380.276**
2	308.821	320.033	331.200	345.600	390.706
3	316.700	331.769	349.500	362.840	405.623
4	340.500	351.801	365.648	379.820	411.670
5	**358.970**	369.058	387.740	400.270	**425.678**

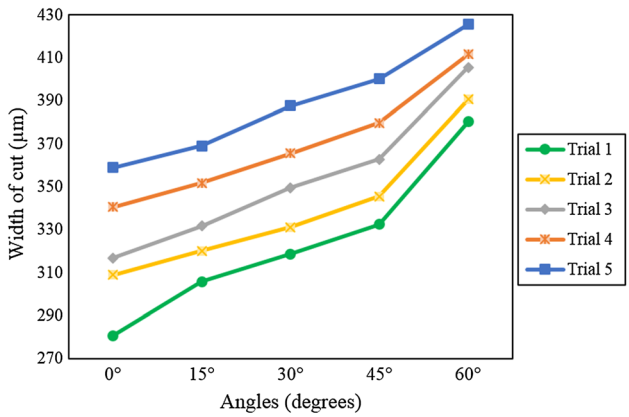

Fig. 10 Variation of width of cut for different angles of cut

using SEM at various angles of cut is as shown in Table 9. Figure 10 shows the variation of the width of cuts at different chosen parameters that were cut at different angles of cut. Figure 11 shows SEM micrograph of the different width of cut at 0°, 15°, 30°, 45°,60° angles of cut at different machining parameters. The width of cut mainly depends on wire vibration, servo voltage, servo feed, amplitude of vibration and job height [19, 22, 27]. The lowest width of cut was recorded in trial 1 which was varying from 280.678 380.276 μm at 0° and 60°, respectively. Trial 1 measured lowest cutting speed with a lower width of cuts as it has the highest servo feed in all angle of cut. However, trial 5 offers the highest width of cut varied from 358.97 to 425.678 μm at 0° and 60°, respectively, and it has the least servo feed with the highest cutting speed. During sparking, if the servo feed is least the distance of wire movement inside the material is reduced. This makes a larger width of cut as the material around the wire is exposed to sparking for a longer time than the normal cutting [22, 27]. The highest width of cut was observed at 60° for all the trials, and for all the individual machining parameters the width of cut increases with increase in the angle of cut. As cutting thickness increases the amplitude of wire vibration also increases; hence, it increases the width of cut [19, 22]. In all the trials, the width of cut increased, but there was a noticeable increase in the width of cut for 45° and 60° as shown in Fig. 10. This behaviour is due to the rapid increase in the cutting thickness from 15.56 to 20 mm, which in turn increases the amplitude of wire vibration as stated by Abhishek et al. [19].

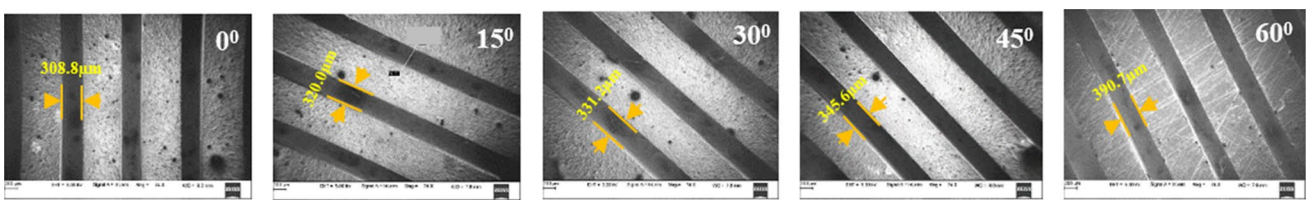

Fig. 11 SEM images of slant cut at 0°,15°,30°,45° and 60°

4 Conclusion

Hastelloy X a nickel-based superalloy was employed for angular machining using WEDM. The angularity in machining was achieved with the aid of slant type taper fixture which removes many flaws like wire break, angular error, guide wear and surface flaws in taper machining. Different cutting speeds were considered from 0.16 to 2.49 mm/min for investigation of various output parameters like taper angle, surface roughness, surface crack density and width of cut at various angles in WEDM. The variation in cutting speed with the angle of cut was reported in the present work. The following conclusions were drawn from the experimental results.

1. The cutting speed decreased with an increase in angle of cut, and there was the highest reduction of 65.57% in cutting speed observed from 2.49 to 0.85 mm/min at 60° slant angle due to the increase in cutting thickness.
2. The trial 5 (pulse on time = 125, servo voltage = 40, wire feed = 8, servo feed = 15) was observed to have a maximum of − 29′27″ at 15° and minimum − 0′53″ at 60° errors among all the angle of cut due to higher stochastic vibrational amplitude and manufacturing errors.
3. The surface roughness was observed to be 1.73 µm at lowest cutting speed (0.16 mm/min) with 60° slant angle, and at highest cutting speed (2.49 mm/min) the surface roughness is recorded to be 3.57 µm at 0°. The highest surface roughness was recorded as 3.99 µm at 60° angle of cut having cutting speed as 0.85 mm/min, due to the increase in cutting thickness.
4. The highest surface crack density was calculated to be 0.455 µm/µm^2 at 60° angle of cut having the low cutting speed of 0.85 mm/min, due to the increase in cutting thickness. The highest increase in surface crack density was observed in cutting speed of 38.72% at 60° and followed by 34.81% at 45° slant angle.
5. The width of cut was found to be increasing with an increase in angle of cut, and it was noticeable prominently at 45° and 60° due to 28.53% increase in cutting thickness. The highest increase in the width of cut was observed to be 14.41% from 45° and 60° slant angles at lowest cutting speeds with the highest servo feed and high vibrational amplitude for trial 1.

References

1. Choudhury, I.A.; El-Baradie, M.A.: Machinability of nickel-base super alloys: a general review. J. Mater. Process. Technol. **77**, 278–284 (1998)
2. Benjamin, J.S.: Dispersion strengthened super alloys by mechanical alloying. Metall. Trans. B. **1**, 2943–2951 (1970)
3. Ezugwu, E.O.; Wang, Z.M.; Machado, A.R.: The machinability of nickel-based alloys: a review. J. Mater. Process. Technol. **86**, 1–16 (1999)
4. Han, F.; Kunied, M.; Sendai, T.; Imai, Y.: High precision simulation of WEDM using parametric programming. CIRP Ann. **51**, 165–168 (2002)
5. Shihab, S.K.: Optimization of WEDM process parameters for machining of friction-stir-Welded 5754 aluminum alloy using Box–Behnken design of RSM. Arab. J. Sci. Eng. **43**(9), 5017–5027 (2018)
6. Goswami, A.; Kumar, J.: Optimization in wire-cut EDM of Nimonic-80A using Taguchi's approach and utility concept. Eng. Sci. Technol. Int. J. **17**, 236–246 (2014)
7. Soni, H.; Narendranath, S.; Ramesh, M.R.: Effects of wire electro-discharge machining process parameters on the machined surface of $Ti_{50}Ni_{49}Co_1$ shape memory alloy. Silicon-Neth. **11**(2), 733–739 (2019)
8. Zhang, Z.; Ming, W.; Huang, H.; Chen, Z.; Xu, Z.; Huang, Y.; Zhang, G.: Optimization of process parameters on surface integrity in wire electrical discharge machining of tungsten tool YG15. Int. J. Adv. Manuf. Technol. **81**, 1303–1317 (2015)
9. Selvakumar, G.; Jiju, K.B.; Veerajothi, R.: Experimental study on wire electrical discharge machining of tapered parts. Arab. J. Sci. Eng. **41**, 4431–4439 (2016)
10. Martowibowo, S.Y.; Wahyudi, A.: Taguchi method implementation in taper motion wire EDM process optimization. J. Inst. Eng. India Ser. C **93**, 357–364 (2010)
11. Kinoshita, N.; Fukui, M.; Fujii, T.: Study on wire-EDM: accuracy in taper-cut. CIRP. Ann-Manuf. Technol. **36**, 119–122 (1987)
12. Plaza, S.; Ortega, N.; Sanchez, J.A.; Pombo, I.; Mendikute, A.: Original models for the prediction of angular error in wire-EDM taper-cutting. Int. J. Adv. Manuf. Technol. **44**, 529–538 (2009)
13. Sanchez, J.A.; Plaza, S.; Ortega, N.; Marcos, M.; Albizuri, J.: Experimental and numerical study of angular error in wire-EDM taper-cutting. Int. J. Mach. Tool. Manuf. **48**, 1420–1428 (2008)
14. Sanchez, J.A.; Plaza, S.; Lacalle, L.N.L.D.; Lamikiz, A.: Computer simulation of wire-EDM taper-cutting. Int. J. Comput. Integr. Manuf. **19**, 727–735 (2006)
15. Yan, H.; Liu, Z.; Li, L.; Li, C.; He, X.: Large taper mechanism of HS-WEDM. Int. J. Adv. Manuf. Technol. **90**, 2969–2977 (2017)
16. Chandler, H.: Heat Treater's Guide Practices and Procedures for Nonferrous Alloys. Third Printing (2006).
17. Sharma, P.; Chakradhar, D.; Narendranath, S.: Evaluation of WEDM performance characteristics of Inconel 706 for turbine disk application. Mater. Des. **88**, 558–566 (2015)
18. Ishfaq, K.; Mufti, N.A.; Mughal, M.P.; Saleem, M.Q.; Ahmed, N.: Investigation of wire electric discharge machining of stainless-clad steel for optimization of cutting speed. Int. J. Adv. Manuf. Technol. **96**, 1429–1443 (2018)
19. Samanta, A.; Sekh, M.; Sarkar, S.: Influence of different control strategies in wire electrical discharge machining of varying height job. Int. J. Adv. Manuf. Technol. **100**(5–8), 1299–1309 (2016)
20. Azam, M.; Jahanzaib, M.; Ali Abbasi, J.; Wasim, A.: Modeling of cutting speed (CS) for HSLA steel in wire electrical discharge machining (WEDM) using moly wire. J. Chin. Inst. Eng. **39**(7), 807–808 (2018)
21. Rabinovich, S.G.: Measurement Errors and Uncertainties. Theory and Practice, 3rd edn. Springer, New York (2006)
22. Habib, S.: Optimization of machining parameters and wire vibration in wire electrical discharge machining process. Int. J. Adv. Manuf. Technol. **3**(3), 1–9 (2017)
23. Habib, S.; Okada, A.: Experimental investigation on wire vibration during fine wire electrical discharge machining process. Int. J. Adv. Manuf. Technol. **84**, 2265–2276 (2016)

24. Puri, A.B.; Bhattacharyya, B.: Modelling and analysis of the wire-tool vibration in wire-cut EDM. J. Mater. Process. Technol. **141**, 295–301 (2003)
25. Kumar, V.; Kumar, V.; Jangra, K.K.: An experimental analysis and optimization of machining rate and surface characteristics in WEDM of Monel-400 using RSM and desirability approach. J. Ind. Eng. Int. **11**, 297–307 (2015)
26. Kumar, A.; Kumar, V.; Kumar, J.: Surface crack density and recast layer thickness analysis in WEDM process through response surface methodology. Mach. Sci. Technol. **20**, 201–230 (2016)
27. Chen, Z.; Zhang, G.; Han, F.; Zhang, Y.; Rong, Y.: Determination of the optimal servo feed speed by thermal model during multi-pulse discharge process of WEDM. Int. J. Mech. Sci. **142–143**, 359–369 (2018)